Macromolecules

ARTICLE

pubs.acs.org/Macromolecules

Diameter-Dependent Modulus and Melting Behavior in Electrospun Semicrystalline Polymer Fibers

Ying Liu,*[,†] Shuang Chen,[†] Eyal Zussman,[‡] Chad S. Korach,[§] Wei Zhao,[§] and Miriam Rafailovich[†]

[†]Department of Material Science and Engineering, Stony Brook University, Stony Brook, New York 11794-2275, United States

[‡]Department of Mechanical Engineering, Technion-Israel Institute of Technology, Haifa 32000, Israel

[§]Department of Mechanical Engineering, Stony Brook University, Stony Brook, New York 11794-2300, United States

ABSTRACT: Confinement of the semicrystalline polymers, poly(ethylene-*co*-vinyl acetate) (PEVA) and low-density polyethylene (LDPE), produced by electrospinning has been observed to produce fibers with large protrusions, which have not been previously observed in fibers of comparable diameters produced by other methods. SAXS spectra confirmed the crystalline structure and determined that the lamellar spacing was almost unchanged from the bulk. Measurement of the mechanical properties of these fibers, by both shear modulation force microscopy (SMFM) and atomic force acoustic microscopy (AFAM), indicates that the modulii of these fibers increases with decreasing diameter, with the onset at ~10 μm, which is an order of magnitude larger than previously reported. Melting point measurements indicate a decrease of more than 7% in T_m/T_0 (where T_m is the melting point of semicrystalline polymer fibers and T_0 is the melting point of the bulk polymer) for fibers ranging from 4 to 10 μm in diameter. The functional form of the decrease followed a universal curve for PEVA, when scaled with T_0.

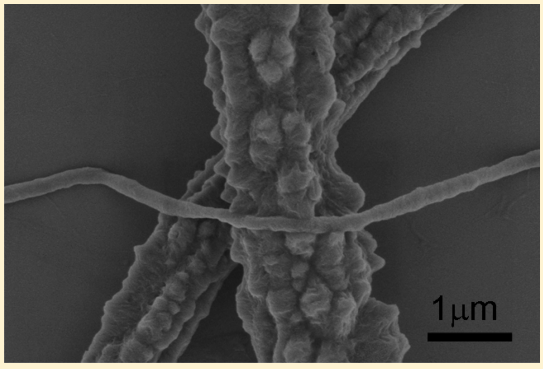

1. INTRODUCTION

The study of the polymers in structurally confined environment is a topic of increasing interest since polymer chains have multiple degrees of freedom, and confinement alone can impart special properties.[1] Polymer-based fibers, often being called materials with reduced dimension, have attracted much attention recently because of their unique mechanical and thermodynamic properties.[2] For example, in amorphous polymer fibers, an increase in the modulii was reported, which scaled inversely with decreasing fiber diameter.[3,4] Later, this increase was shown to be a universal phenomenon and, in the case of monodisperse polymers, scaled with radius of gyration (R_g) of the polymer molecules.[5] The latter result was particularly surprising, since no change in the glass transition temperature (T_g) was observed, and the measuring temperature was lower than T_g, where no molecular weight effect on the modulus had previously been reported. Consequently, this phenomenon was attributed to confinement induced chain orientation during the spinning process, where the molecules were still mobile within the concentrated spinning solution stream.

Morphological constraints are even more important in determining the properties of semicrystalline polymers, where the nature of the crystals is known to determine the mechanical and thermodynamic properties. Numerous studies exist on the effects of confinement on two-dimensional (2D) semicrystalline thin films.[6−14] The degree of confinement is even greater in the fibrillar geometry, but the complexity of making these fibers has thwarted some of the research efforts.[15,16] Most work to date involves drawn fibers, which are limited to tens of micrometers in size.[15,17,18] Electrospinning, which can produce nanoscale fibers, is very difficult since crystallization interferes with the fiber formation process.[19−21] Recently, Givens et al. have shown that polyethylene (PE) can be spun into fibers if the solution is heated using infrared light.[20] Here we use a method that further facilitates the process and allows for temperature control of the spinning solution. This has allowed us to electrospin larger quantities of fiber samples and enabled us to study the structure/property relationships of the fibers with a variety of complementary techniques. Since a great deal is already known about the bulk crystalline properties of PE, we could then determine which effects are due to confinement.

2. MATERIALS AND METHODS

2.1. Materials. Poly(ethylene-*co*-vinyl acetate) (PEVA) was purchased from Dupont Co. with the commercial name Elvax 260 (PEVA260), Elvax 550 (PEVA550), and Elvax 750 (PEVA750), separately. The low-density polyethylene (LDPE) was purchased from Flint Hills Resources. *p*-Xylene and tetrabutylammonium chloride (TBAC) were purchased from Sigma-Aldrich. Chloroform was purchased from Fisher Science.

2.2. Electrospinning of PEVA and LDPE Fibers. To prepare electrospun polymer fibers, PEVA and LDPE with different weight

Received: February 5, 2011
Revised: April 10, 2011
Published: May 10, 2011

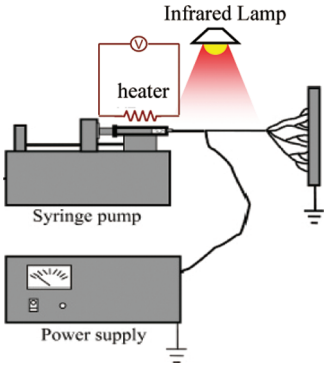

Figure 1. Schematic of the electrospinning apparatus. The polymer solution was loaded in the syringe. A high voltage of 10 kV was applied between the needle and the collector. The flow rate was 50 μL/min.

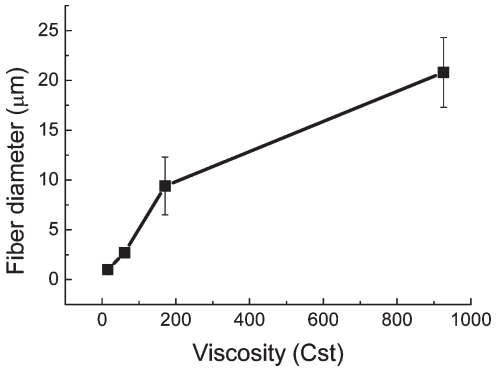

Figure 2. Diameters of electrospun PEVA260 fibers vs electrospinning solution viscosity.

concentration were dissolved in chloroform and *p*-xylene, respectively. The solutions were left at room temperature overnight and then heated on a hot plate until the solution completely dissolved. PEVA solutions were electrospun directly, while 0.2 wt % of TBAC was added into LDPE electrospnning solution. The experimental setup is shown in Figure 1. In the electrospinning process, 3 mL of the solution was drawn into the 5 mL glass syringe (Hamilton Co., Reno, NV) that was then secured onto the graduated pump (KD Scientific, Holliston, MA), and the flow rate was set to be 50 μL/min. The high-voltage power supply (Gamma High Voltage Research, Ormond Beach, FL) was set to 10 kV and attached to the needle. Because of the relatively poor solubility of PEVA and PE in conventional solvent system at ambient temperature, a heating system was appended to the conventional electrospinning setup: (1) A flexible Kapton tape heater was attached the syringe and wrapped around the barrel and needle, in order to control solution temperature during electrospinning and the Taylor cone. The heating temperature was adjusted according to the melting point of different polymers. The solution temperature was maintained at 78, 96, 104, and 114 °C for PEVA260, PEVA550, PEVA750, and PE, respectively. (2) An infrared lamp was also used to maintain the elevated temperature between the spinner and collector. Electrospun fibers were collected on cleaned aluminum foils or silicon wafers as randomly oriented fiber mat on the aluminum target, which was horizontally placed 10 cm away from the tip of the needle. The electrospun fibers were then placed in a vacuum oven, at 25 °C overnight, in order to remove residual solvent.

2.3. Characterization of PEVA Fibers. *Imaging.* The morphologies of the fibers were imaged by using scanning electron microscopy (SEM, LEO 1550, LEO, Germany) with 2.5 kV acceleration voltage and at working distance of 2−4 cm. All fiber samples were sputter-coated with gold to improve the surface conductivity. The fiber diameter distributions of PEVA and LDPE fibers were obtained by analyzing the SEM image with Image Tool (The University of Texas, Health Science Center in San Antonio).

Solution Viscosity Measurement. For PEVA260, the viscosity of the solutions prepared for electrospinning was measured using by a KV 4000 viscometer (Koehler Instrument Co., New York). In Figure 2 we plot the fiber diameters, as determined by SEM, versus the solution viscosity and find that it increases monotonically, which is in agreement with previous observations.[22]

Small-Angle X-ray Scattering (SAXS). SAXS measurements for PVEA and LDPE fibers and bulk materials were carried out at the X10A beamline of National Synchrotron Light Source (NSLS), Brookhaven National Laboratory (BNL), using a photon energy 11.3 keV, i.e., X-ray wavelength (λ) of 10.9 Å.

Measurement of the Stiffness. Relative modulus of the electrospun fibers were measured by a Veeco/DI Dimension 3000 atomic force microscope (AFM). The principle of the shear modulation force microscopy (SMFM) method and the setup of the experiment were described in an earlier article.[23] When the drive signal amplitude was varied from 7.5 to 125 mV, which corresponded to an *x*-piezo displacement of 1.5−25 nm, the cantilever response was recorded to estimate the stiffness of the fibers. At least three fibrils were measured for the same diameter of the same materials. Each fiber was measured at least three locations. Three measurements were done at each location. Hence, the data represented an average of 27 measurements.

Measurements of the mechanical properties of the PEVA fibers were also performed by the atomic force acoustic microscopy technique (AFAM) since the SMFM method, described above, is sensitive to the surface of the fiber, while the AFAM method is sensitive to the entire fiber, due to the long wavelength of the acoustic probe.

A conventional atomic force microscope (NT-MDT SolverProM) was used with the sample mounted on an ultrasonic transducer which emits longitudinal acoustic waves.[24] The AFM cantilever is brought into contact with the sample, and the resulting vibrational frequencies in the cantilever were measured with the laser−photodiode system. The AFAM technique has successfully been used to measure the elastic modulus of thermoset epoxies.[25] The tip−sample contact stiffness is modeled as a linear spring, and using a cantilever beam model the equations of motion can be solved analytically if amplitudes are kept sufficiently small, yielding the contact stiffness as a function of vibrational frequency. An AFM cantilever (AIST fpN11S) with spring constant of 6.1 N/m, calibrated by the thermal tuning method,[26] was used for all measurements. An indium film was used to calibrate the AFM cantilever and determine the tip radius of curvature. A normal load of 1 μN was applied by the cantilever to the tip−substrate interface through the cantilever bending calibration. Fibers were distributed randomly on a silicon substrate that was then mounted on the ultrasonic transducer with a small volume of honey which is allowed to set for at least 1 h. The built-in zoom microscope was used to identify fibers of interest and measure fiber widths. Small diameter fibers (<7 μm) were imaged directly with the AFM in a semicontact (tapping) mode, and AFAM measurements were made at the apex of the fiber. For larger diameter fibers, the AFM tip was landed directly on the fiber and the surface imaged to determine the location of the apex. At least four AFAM measurements were performed on each fiber size.

Measurement of the Melting Point. The melting point (T_m) of bulk materials was measured by differential scanning calorimetry (DSC), which was conducted in air at a heating rate of 5 °C/min in the temperature range between ambient temperature and 100 °C using a Netzsch STA 499C thermal analyzer. The bulk materials were first dissolved in the spinning solution and dried for 3 days. Then samples weighing ~5 mg were loaded in a SiO_2 crucible under dry conditions.

Table 1. Weight Percent (wt %) of Ethylene, Density, and Melting Point (Measured by DSC) of PEVA260, 550, 750, and LDPE

sample	wt % of ethylene	density, g/cm^3	melting point (DSC), °C
Elvax260	72	0.955	78
Elvax550	85	0.935	96
Elvax750	90	0.93	104
LDPE	100	0.924	114

The melting point (T_m) of the electrospun fibers was measured by using a Veeco/Digital Instruments Dimension 3000 atomic force microscopy (AFM) located in a sealed glovebox purged with dry nitrogen.[14,27] The same etched silicon cantilever (Digital Instruments) with a spring constant of ~0.1 N/m was used for all measurements. In this method, a sinusoidal drive signal with a frequency of 1400 Hz was applied to the x-piezo controlling the cantilever, inducing a small oscillatory motion of the tip parallel to the sample surface. A normal load force of 25 nN was applied to the tip which produced an indentation, h, into the sample. The lateral deflection amplitude, Δx, was measured as the output, which has the following relationship with the lateral modulus of the fibers: $\Delta x \propto G^{-2/3}$. The electrospun fibers on cleaned silicon wafers were mounted on a heating/cooling stage (MMR Technologies) for melting point measurement. Since G decreases by orders of magnitude when the fiber melts at T_m, the signal has a strong and sharp transition.

3. RESULTS AND DISCUSSION

3.1. Melting Temperature Depression of PEVA and LDPE Fibers. We had previously observed a decrease in the melting point with decreasing fiber diameter for electrospun fibers of semicrystalline PEVA260 polymers.[27] In Table 1, we list the ethylene fraction of different PEVA copolymers, and we can see that the PEVA260 polymer has the largest fraction of acetate and is known to have the lowest degree of crystallinity. Therefore, it was difficult to draw quantitative conclusions from those data alone, without studying the dependence of T_m as a function of the PE content. Hence, we extended the study, using the same technique, SMFM, described preciously,[14,27] to measure T_m as a function of both fiber diameter and PE fraction. The amplitude of the modulation is inversely proportional to the modulus, and hence the abrupt rise in amplitude signifies the abrupt decrease (3 orders of magnitude) which occurs upon melting of the sample. From the figures, we can see that, even though the transition occurs at different temperatures for the various polymers, within a given polymer series, the transition occurs at progressively lower temperatures with decreasing fiber diameter (Figure 3a−c).

The melting point of the bulk polymer, T_0, is known to depend on the amorphous fraction. We therefore measured T_0 for the bulk polymer independently using DSC. The results are listed in Table 1, where we find that T_0 decreases with decreasing ethylene fraction. We then scaled the T_m values for each polymer with the melting point of the bulk polymer, T_0, and replotted the results in Figure 3d, where we find that for the PEVA series of polymers the values all appear to lie on a universal curve, where T_m/T_0 decreases by almost 20% as the diameter of the fibers decreases from 12 to 4 μm. Hence, the melting point depression is not a function of the degree of crystallinity or the fraction of amorphous copolymer. A similar response is also observed for

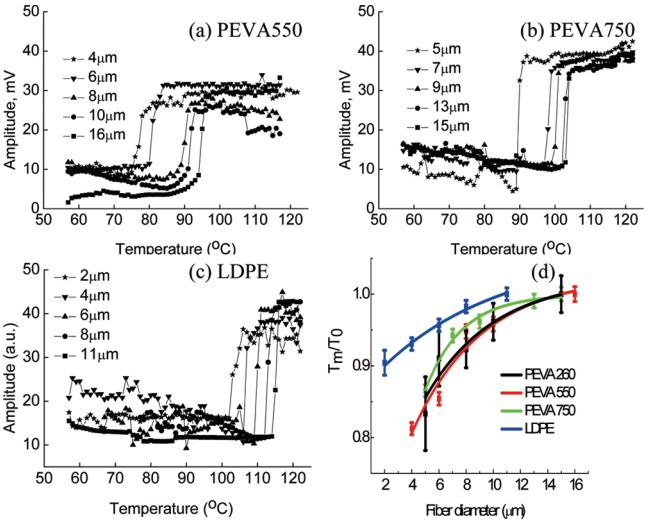

Figure 3. Deflection amplitude of the cantilever (Δx) versus temperature for (a) PEVA260, (b) PEVA750, and (c) LDPE electrospun fibers. (d) The melting point, T_m, as measured by SMFM, and scaled by the bulk value, T_0, versus the fiber diameter for PEVA260, 550, 750, and LDPE fibers.

the pure LDPE sample, where a more gradual decrease of about 7% is observed in this region.

A decrease in T_m is predicted by the Thomson−Gibbs equation[28,29]

$$T_m = T_m^0 - \frac{2\gamma_e T_m^0}{l\Delta H_v} \quad (1)$$

where T_m^0 is the melting point for the infinitely large crystal, γ_e is the top and bottom surface energy of the crystal lamellae, ΔH_v is the heat of fusion, and l is the lamellae thickness. In this case, T_m is reduced if the confinement is such that the lamellar thickness is reduced. We had previously measured l for PEVA260, where the largest decrease is observed, and found l = 22 nm,[27] which is the same as the value obtained for bulk PEVA260. Hence, this mechanism cannot be applied. Wang et al. reported a depression of comparable magnitude in the melting point of LDPE films. The onset of the depression occurred for films 150 nm or thinner,[14] which was also much larger than l, but still an order of magnitude smaller than the diameter of the fibers in this study. X-ray scattering of the LDPE samples also indicated bulklike values of l, but in the region where the depression occurred, they observed reorientation of the lamellae parallel to the substrate surface.[30,31] Hence, they attributed their effects to surface interactions.

It has recently been proposed by Arinstein et al.[32] that the depression of the melting point with polymer diameter may be related to the initial viscosity of the spinning solution. As was shown preciously in Figure 2, the fiber diameters are controlled by varying the polymer concentration and hence the viscosity of the solution. The concentrations listed above are all relatively high and form entangled networks which are distorted by the high shear produced in the spinning process. Because of fast solvent evaporation, fixation of topological structure of the polymer matrix occurs in a nonequilibrium conformation, where the degree of chain entanglement is lower than that in polymer bulk at equilibrium. This difference results in an additional entropy term, resulting in a reduction of the melting point as

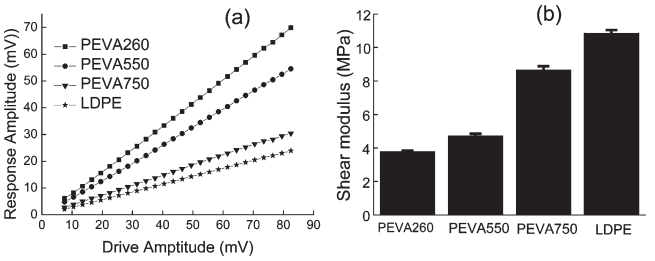

Figure 4. Shear modulus dependence on crystallinity for PEVA260, 550, 750, and LDPE electrospun fibers with fiber diameter of 4 μm. For the same fiber diameter, modulus increases with increasing crystallinity.

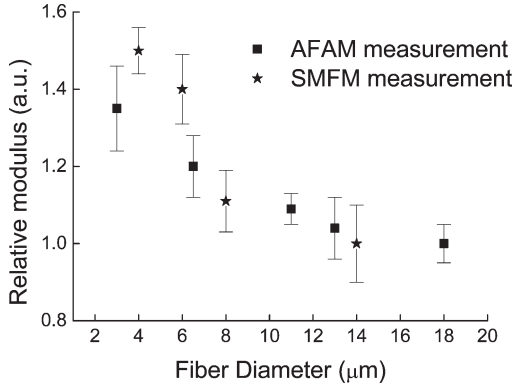

Figure 5. Relative modulus of electrospun PEVA260 fibers measured by two different methods: AFAM and SMFM method.

residual stress relaxation occurs differentially for different fiber diameters.

3.2. Relationship between Mechanical Properties and Crystallinity. We can now compare the effect of the degree of crystallinity on the modulus of the fibers at ambient temperature. In Figure 4 we plot the modulus of fibers of fixed diameter, 4 μm, as a function of the ethylene content. From the figure, we see that the modulus increases as the ethylene fraction increases, which is not surprising since the bulk modulus of LDPE is ~1.5 times larger than that of poly(vinyl acetate).[33]

If we keep the ethylene content fixed, we can also compare the effect of fiber diameter on the modulus. In Figure 5 we plot the values of PEVA260, which were measured by two separate, but complementary, techniques. From the figure we can also clearly see that the modulii increase by 40% as the fiber diameters decrease from 18 to 2 μm. A similar increase in modulus with decreasing fiber diameter was previously reported by Zussman et al.[4] In their systems, the onset occurred for diameter below 1 μm, in contrast to the PEVA260 systems where the onset occurs for diameters less than 10 μm. This observation seems to confirm their interpretation of the results as being due to supramolecular structures internal to the fibers, rather than surface induced alignment, since it is very difficult to explain surface orientation propagating into the interior of the fibers for these larger distances.

In order to establish that the increased modulus occurs throughout the entire fiber, we also measured the moduli using the AFAM method. The relative moduli obtained by AFAM and SMFM are plotted together in Figure 5, where we find that the results are in good agreement, indicating that the increased modulus with decreasing fiber diameter is characteristic of the fiber and is not simply a surface phenomenon.

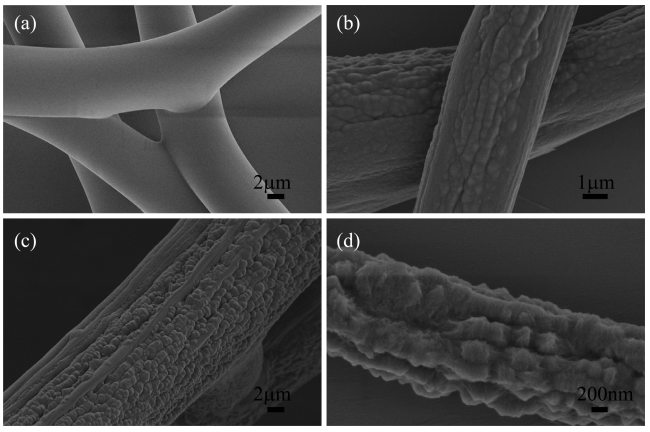

Figure 6. SEM images of electrospun (a) PEVA260, (b) PEVA550, (c) PEVA750, and (d) LDPE fibers.

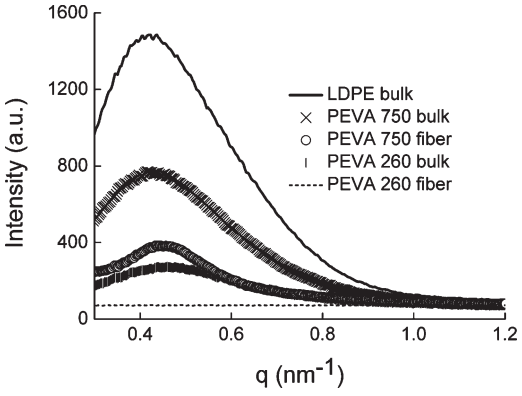

Figure 7. SAXS of LDPE, PEVA750, PEVA260 bulk materials and PEVA750, PEVA260 fibers.

3.3. Surface Morphologies of Electrospun PEVA and LDPE Fibers. Figure 6 shows SEM images of the fiber morphologies electrospun from different polymers. From the figure we can see that in the case of PEVA260 the fiber surfaces are smooth, while rough, angular features are seen to develop on electrospun PEVA550, 750, and LDPE fibers. From the figures we can also see that these features appear to be aligned in rows running parallel to the fiber axis, and their magnitude increases with increasing PE content or decreasing acrylate fraction in the polymer. We therefore propose that these features are due to rapid crystallization which forms along the stream lines of the fibers.

In order to ensure that the features were not due to adsorbed organic salts used as viscosity modifiers in the electrospinning solution, some of the samples were also soaked in the spinning solution after they were formed in order to dissolve the salts. No change in surface morphology was observed, confirming that the surface morphology was due to the structures of the polymers themselves.

We also performed SAXS on these fibers, and the spectra obtained from bulk and fiber samples, together with PE bulk data, are shown in Figure 7. From the figure, we can see that the peak position for the EVA750 copolymer is the same as that of the LDPE bulk sample, confirming that the crystalline structures are primarily due to the PE content. Furthermore, the position of the scattering peak of the fiber and bulk samples are similar for

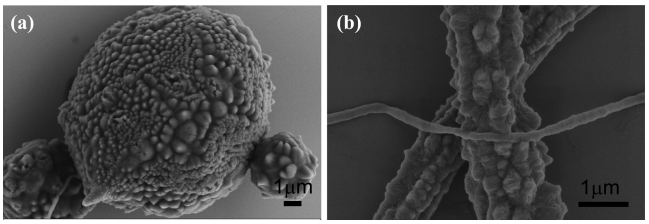

Figure 8. SEM images of electrospun LDPE (a) bead and (b) fibers.

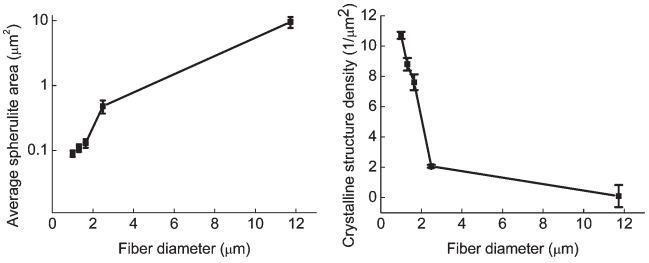

Figure 9. Analysis of crystalline structures as a function of fiber diameter on electrospun LDPE fibers: (a) average area and (b) average density.

PEVA750, indicating that no change in lamellar spacing occurs during the spinning process. In the case of PEVA260 a small peak is observed for the bulk sample, but the peak is too small to analyze for the fiber sample. This observation is consistent with the large features observed on PEVA750 fibers and near lack of features on the PEVA260 fibers.

On LDPE fibers, we can study the crystalline structures in more detail, since no amorphous component is present to modulate the features. The result is shown in Figure 6d where we can see that distinct crystalline features form along long furrows that follow the contour of the fiber. These features have not been observed for drawn LDPE fibers of comparable diameters.[34] In the drawing process, solvent evaporation occurs relatively slowly under controlled conditions. In the electrospinning process, solvent evaporation occurs abruptly, leading to rapid crystallization. The alignment of the features may result from crystallization along the streamlines which are set up in the jet during the spinning process.

In Figure 8a, we show a SEM image of the PE electrospun beads, which have been reported by numerous authors and has been attributed to turbulence in the polymer solution.[35] When turbulence arises and bead formation results, the furrow lines are observed to stop abruptly, and crystallite structures are formed along the contour of the beads. In Figure 8b we show fibers of different diameters where we can see that for fibers approximately 1 and 1.5 μm in diameter smooth regions coexist with those that have crystalline structures, and for fibers less than 0.2 μm, no crystalline structures are observed.

We can then measure both the amount of crystalline structure, and the area per crystalline structure, as a function of fiber diameter. The results are plotted in Figure 9, where we see a sharp increase with decreasing diameters below 2 μm. Hence, electrospun fibers from crystalline polymers are seen to exhibit unusual surface morphologies which have not been reported before on drawn fibers of the same diameter and whose magnitude appears to be related to the degree of crystallinity of the bulk material.

4. CONCLUSIONS

Since polymeric chains have multiple degrees of freedom, confinement alone can impart special properties. In this paper, we reported that in semicrystalline polymers, such as PEVA and LDPE, confinement brought by electrospinning can change the melting point while at the same time improving the mechanical properties. SEM analysis of the electrospun semicrystalline polymer fibers shows that microcryslline protrusions appear on the surface of fibers thicker than 200 nm. These protrusions are not apparent on drawn fibers of the same diameters, and they appear to be ordered along flow lines in the fibers. The protrusions also increase in size with increasing LDPE fraction. The protrusions are unique to electrospun fibers and have not been observed in mechanically drawn fibers.

■ ACKNOWLEDGMENT

We gratefully acknowledge the financial support of the NSF-MRSEC program and discussions with Prof. Gad Marom of the Hebrew University, Jerusalem, Israel.

■ REFERENCES

(1) Kassner, M. E.; Nemat-Nasser, S.; Suo, Z. G.; Bao, G.; Barbour, J. C.; Brinson, L. C.; Espinosa, H.; Gao, H. J.; Granick, S.; Gumbsch, P.; Kim, K. S.; Knauss, W.; Kubin, L.; Langer, J.; Larson, B. C.; Mahadevan, L.; Majumdar, A.; Torquato, S.; van Swol, F. *Mech. Mater.* **2005**, *37* (2−3), 231–259.

(2) Saheb, D. N.; Jog, J. P. *Adv. Polym. Technol.* **1999**, *18* (4), 351–363.

(3) Ji, Y.; Li, B. Q.; Ge, S. R.; Sokolov, J. C.; Rafailovich, M. H. *Langmuir* **2006**, *22* (3), 1321–1328.

(4) Arinstein, A.; Burman, M.; Gendelman, O.; Zussman, E. *Nature Nanotechnol.* **2007**, *2* (1), 59–62.

(5) Ji, Y.; Li, C.; Wang, G.; Koo, J.; Ge, S.; Li, B.; Jiang, J.; Herzberg, B.; Klein, T.; Chen, S.; Sokolov, J. C.; Rafailovich, M. H. *EPL* **2008**, *84* (5), xxxx.

(6) Reiter, G.; Sommer, J. U. *Phys. Rev. Lett.* **1998**, *80* (17), 3771–3774.

(7) Despotopoulou, M. M.; Frank, C. W.; Miller, R. D.; Rabolt, J. F. *Macromolecules* **1996**, *29* (18), 5797–5804.

(8) Schonherr, H.; Frank, C. W. *Macromolecules* **2003**, *36* (4), 1188–1198.

(9) Mellbring, O.; Oiseth, S. K.; Krozer, A.; Lausmaa, J.; Hjertberg, T. *Macromolecules* **2001**, *34* (21), 7496–7503.

(10) Reiter, G.; Sommer, J. U. *J. Chem. Phys.* **2000**, *112* (9), 4376–4383.

(11) Sommer, J. U.; Reiter, G. *J. Chem. Phys.* **2000**, *112* (9), 4384–4393.

(12) Zhang, F.; Liu, J.; Huang, H.; Du, B.; He, T. *Eur. Phys. J. E* **2002**, *8* (3), 289–297.

(13) Bartczak, Z.; Argon, A. S.; Cohen, R. E.; Kowalewski, T. *Polymer* **1999**, *40* (9), 2367–2380.

(14) Wang, Y.; Ge, S.; Rafailovich, M.; Sokolov, J.; Zou, Y.; Ade, H.; Luning, J.; Lustiger, A.; Maron, G. *Macromolecules* **2004**, *37* (9), 3319–3327.

(15) Peterlin, A. *Colloid Polym. Sci.* **1987**, *265* (5), 357–382.

(16) Kulkarni, J. A.; Beris, A. N. *J. Non-Newtonian Fluid Mech.* **1999**, *82* (2−3), 331–366.

(17) Pennings, A. J.; Smook, J.; Deboer, J.; Gogolewski, S.; Vanhutten, P. F. *Pure Appl. Chem.* **1983**, *55* (5), 777–798.

(18) Schellekens, R.; Bastiaansen, C. *J. Appl. Polym. Sci.* **1991**, *43* (12), 2311–2315.

(19) Stephens, J. S.; Chase, D. B.; Rabolt, J. F. *Macromolecules* **2004**, *37* (3), 877–881.

(20) Givens, S. R.; Gardner, K. H.; Rabolt, J. F.; Chase, D. B. *Macromolecules* **2007**, *40* (3), 608–610.
(21) Rein, D. M.; Shavit-Hadar, L.; Khalfin, R. L.; Cohen, Y.; Shuster, K.; Zussman, E. *J. Polym. Sci., Part B: Polym. Phys.* **2007**, *45* (7), 766–773.
(22) Baumgart, Pk. *J. Colloid Interface Sci.* **1971**, *36* (1), 71.
(23) Ge, S.; Pu, Y.; Zhang, W.; Rafailovich, M.; Sokolov, J.; Buenviaje, C.; Buckmaster, R.; Overney, R. M. *Phys. Rev. Lett.* **2000**, *85* (11), 2340–2343.
(24) Rabe, U.; Amelio, S.; Kester, E.; Scherer, V.; Hirsekorn, S.; Arnold, W. *Ultrasonics* **2000**, *38* (1−8), 430–437.
(25) Zhao, W.; Singh, R. P.; Korach, C. S. *Composites, Part A* **2009**, *40* (5), 675–678.
(26) Hutter, J. L.; Bechhoefer, J. *Rev. Sci. Instrum.* **1993**, *64* (11), 3342–3342.
(27) Liu, Y.; Li, C. H.; Chen, S.; Wachtel, E.; Koga, T.; Sokolov, J. C.; Rafailovich, M. H. *J. Polym. Sci., Part B: Polym. Phys.* **2009**, *47* (24), 2501–2508.
(28) Wunderlich, B. *Macromolecular Physics*; Academic Press: New York, 1973.
(29) Mandelkern, L. *Crystallization of Polymers*; McGraw-Hill: New York, 1984.
(30) Hershkovits-Mezuman, A.; Harel, H.; Wang, Y. T.; Li, C. H.; Sokolov, J. C.; Rafailovich, M. H.; Marom, G. *Composites, Part A* **2010**, *41* (9), 1066–1071.
(31) Wang, Y. T.; Zou, Y.; Araki, T.; Jan, L. N.; Kilcoyne, A. L. D.; Sokolov, J.; Ade, H.; Rafailovich, M. *Macromolecules* **2010**, *43* (19), 8153–8161.
(32) Arinstein, A. L. Y.; Rafailovich, M.; Zussman, E. *EPL* **2011**accepted.
(33) Lawrence, E. Nielsen, R. F. L. *Mechanical Properties of Polymers and Composites*, 2nd ed.; Marcel Dekker: New York, 1994.
(34) Karlsson, J. O.; Blachot, J. F.; Peguy, A.; Gatenholm, P. *Polym. Compos.* **1996**, *17* (2), 300–304.
(35) Lee, K. H.; Kim, H. Y.; Bang, H. J.; Jung, Y. H.; Lee, S. G. *Polymer* **2003**, *44* (14), 4029–4034.